Cross section and complete set of proton spin observables in $\vec{p}d$ elastic scattering at 250 MeV

K. Hatanaka,[1,*] Y. Shimizu,[1] D. Hirooka,[1] J. Kamiya,[1] Y. Kitamura,[1] Y. Maeda,[2] T. Noro,[3] E. Obayashi,[1] K. Sagara,[3] T. Saito,[2] H. Sakai,[2] Y. Sakemi,[1] K. Sekiguchi,[2] A. Tamii,[2] T. Wakasa,[1] T. Yagita,[3] K. Yako,[2] H. P. Yoshida,[1] V. P. Ladygin,[4] H. Kamada,[5,6] W. Glöckle,[6] J. Golak,[6,7] A. Nogga,[6,8] and H. Witała[7]

[1]*Research Center for Nuclear Physics, Osaka University, Ibaraki, Osaka 567-0047, Japan*

[2]*Department of Physics, University of Tokyo, Bunkyo, Tokyo 113-0033, Japan*

[3]*Department of Physics, Kyushu University, Fukuoka 812-8581, Japan*

[4]*Joint Institute for Nuclear Researches, 141980 Dubna, Russia*

[5]*Department of Physics, Kyushu Institute of Technology, Tobata, Kitakyushu 804-8550, Japan*

[6]*Institut für Theoretische Physik II, Ruhr-Universität Bochum, D-44780 Bochum, Germany*

[7]*M. Smoluchowski Institute of Physics, Jagiellonian University, PL-30059 Kraków, Poland*

[8]*Department of Physics, University of Arizona, Tucson, Arizona 85721*

(Received 11 July 2002; published 9 October 2002)

The angular distributions of the cross section, the proton analyzing power, and all proton polarization transfer coefficients of $\vec{p}d$ elastic scattering were measured at 250 MeV. The range of center-of-mass angles was 10°–165° for the cross section and the analyzing power, and about 10°–95° for the polarization transfer coefficients. These are the first measurements of a complete set of proton polarization observables for $\vec{p}d$ elastic scattering at intermediate energies. The present data are compared with theoretical predictions based on exact solutions of the three-nucleon Faddeev equations and modern realistic nucleon-nucleon potentials combined with three-nucleon forces (3NF), namely, the Tucson-Melbourne (TM) 2π-exchange model, a modification thereof (TM′) closer to chiral symmetry, and the Urbana IX model. Large effects of the three-nucleon forces are predicted. The inclusion of the three-nucleon forces gives a good description of the cross section at angles below the minimum. However, appreciable discrepancies between the data and predictions remain at backward angles. For the spin observables the predictions of the TM 3NF model deviate strongly from the other two 3NF models, which are close together, except for $K_y^{y'}$. In the case of the analyzing power all 3NF models fail to describe the data at the upper half of the angular range. In the restricted measured angular range the polarization transfer coefficients are fairly well described by the TM′ and Urbana IX 3NF models, whereas the TM 3NF model mostly fails. The transfer coefficient $K_y^{y'}$ is best described by the Urbana IX but the theoretical description is still insufficient to reproduce the experimental data. These results call for a better understanding of the spin structure of the three-nucleon force and very likely for a full relativistic treatment of the three-nucleon continuum.

DOI: 10.1103/PhysRevC.66.044002 PACS number(s): 21.45.+v, 21.30.−x, 24.10.−i, 24.70.+s

I. INTRODUCTION

One of the fundamental interests in nuclear physics is to establish the nature of nuclear forces and understand nuclear phenomena based on the fundamental Hamiltonian. Studies of few-nucleon systems offer a good opportunity to investigate these forces. Owing to intensive theoretical and experimental efforts, an often called new generation of realistic nucleon-nucleon (NN) potentials has been obtained using meson-exchange or other more phenomenological approaches, namely, AV18 [1], CD Bonn [2], Nijm I, II, and 93 [3]. They describe the rich set of experimental NN data up to 350 MeV which is well above the pion threshold of 290 MeV. The accuracy of these theoretical predictions is remarkable and can give a χ^2 per degree of freedom very close to 1. These realistic two-nucleon forces (2NF), however, fail to reproduce experimental binding energies for light nuclei where exact solutions of the Schrödinger equation are available, clearly showing underbinding. For instance, the underbinding amounts to 0.5–1 MeV in the case of ^{3}H and ^{3}He and to 2–4 MeV in the case of ^{4}He [4,5]. One can achieve correct three-nucleon ($3N$) and four-nucleon ($4N$) binding energies by including the Tucson-Melbourne (TM) [6,7] or Urbana IX [8] three-nucleon forces (3NF) which are refined versions of the Fujita-Miyazawa force [9], a 2π-exchange between three nucleons with an intermediate Δ excitation. In recent years, it became possible to perform rigorous numerical Faddeev-type calculations for the $3N$ scattering processes by the tremendous advances in computational capabilities [10–12].

In addition to the first signal on 3NF effects resulting from discrete states [13], strong 3NF effects were observed in a study of the minima of the Nd elastic scattering cross section at incoming nucleon energies higher than about 60 MeV [14]. This discrepancy between the data and predictions based exclusively on NN forces could be largely removed by including the 2π-exchange TM 3NF, properly adjusted to reproduce the ^{3}H binding energy in the $3N$ Hamiltonian [14]. This has been confirmed very recently in a new approach based on nuclear forces from chiral perturbation theory [15]. Another theoretical approach for these interme-

*Electronic address: hatanaka@rcnp.osaka-u.ac.jp

diate energies was introduced [16], namely, a coupled channel formalism with Δ-isobar excitation that yields an effective 3NF.

Developments in the technology of ion sources, accelerators, and experimental detection systems enable us to measure a very rich spectrum of spin observables in *Nd* scattering where the incident projectile is polarized and also the polarization of the outgoing particles can be measured. A recent study at RIKEN [17] shows that the inclusion of the 3NF does not always improve the description of precise data taken at intermediate deuteron energies. Proton vector analyzing power data at 70–200 MeV have revealed the deficiency of 3NF's [18,19], which produces large but wrong effects. These results may be caused by a wrong spin structure of present-day 3NF's. Clearly the present situation is only the very beginning of the investigation of the spin structure of the 3NF. In addition, one can expect relativistic effects with increasing energy. A precise measurement of the *nd* total cross section [20,21] revealed that a discrepancy between the data and the 2NF predictions at energies below about 100 MeV could be removed by the inclusion of the TM 3NF. At higher energies this was not the case and the corrections resulting from relativistic kinematics are comparable in size with the 3NF effects. All of the present Faddeev calculations of *Nd* scattering processes with realistic forces are performed in the nonrelativistic framework. Relativistic calculations in many-nucleon systems are an even harder theoretical challenge, although some attempts have already been made [22]. The calculations applied relativistic kinematics, but the Lorentz boost was not taken into account. In the three-body bound system there are some relativistic covariant models [23–26]. We plan to solve directly the relativistic Faddeev 3*N* scattering equation with a Lorentz boosted potential [27–29]. At higher energies, polarization observables, similar to cross sections, will also exhibit 3NF effects as described above. However, the existing higher-energy database for the proton analyzing power is rather poor [30–36]. There are no measurements of two-spin observables except for the spin correlation coefficient C_{yy} at 197 MeV at IUCF [37]. It was pointed out in Ref. [17] that deuteron tensor analyzing powers are difficult to describe with increasing energy by Faddeev calculations including 3NF's. Precise data at intermediate energies including higher-rank spin observables are needed to provide constraints on theoretical 3NF models.

In the present study, we have measured angular distributions of the differential cross section, the analyzing power A_y, and all spin transfer coefficients $K_x^{x'}$, $K_x^{z'}$, $K_z^{x'}$, $K_z^{z'}$, and $K_y^{y'}$ for $\vec{p}d$ elastic scattering at 250 MeV. This energy is slightly above the pion threshold at 215 MeV. Realistic *NN* potentials have been obtained by analyzing the existing *NN* database up to 350 MeV [1–3]. The corresponding proton energy in the *pd* system is 259 MeV to give the same center-of-mass (c.m.) energy. Most of the effects caused by the pion production are expected to be taken into account in the realistic *NN* potentials. The cross section of elastic *pd* scattering shows a smooth energy dependence in the 200–300 MeV range indicating a small effect of the pion production and a possibly larger relativistic effect in this energy region [38].

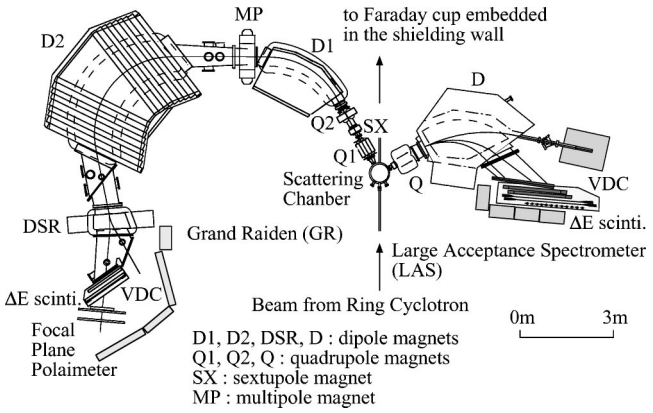

FIG. 1. Schematic layout of the RCNP dual spectrometer consisting of Grand Raiden and LAS.

In Sec. II, we present details of the experimental methods. In Sec. III the 3*N* scattering formalism is summarized and we give a short description of the 3NF's used in this study. In Sec. IV the experimental results are compared with the theoretical predictions. A summary and conclusions follow in Sec. V.

II. EXPERIMENTAL METHODS

The measurements were performed at the Research Center for Nuclear Physics (RCNP), Osaka University using the high resolution spectrometer Grand Raiden [39] including the focal plane polarimeter (FPP) [40] together with the second arm large acceptance spectrometer (LAS) [41]. The experiment was performed during several measurements over a time period of 2 years. Detailed descriptions of the spectrometers and the focal plane polarimeter system can be found in Refs. [39–41]. Here we present only salient details of the experimental setup relevant for the present experiment. The layout of the system is shown in Fig. 1. The proton beam was stopped in a Faraday cup in the scattering chamber for scattering angles smaller than 25.5° in the laboratory frame. For measurements at more backward angles, the beam was transported in a beamline downstream of the scattering chamber and focused by quadrupole magnets into the beam stop and Faraday cup embedded in the shielding wall.

A. Polarized proton beam

Polarized protons were produced in an atomic beam polarized ion source [42], injected into and accelerated by the $K=120$ MeV AVF (azimuthally varying field) cyclotron up to 46.7 MeV. Subsequently the beam was injected into the $K=400$ MeV ring cyclotron [43] and accelerated to the final energy of 250 MeV. The beam polarization was cycled between ''normal'' and ''reverse'' polarization in 10 sec intervals. The polarization axis was vertical ($\hat{y}$) after the AVF cyclotron. Two superconducting solenoids [44] located in the beam transfer line between the AVF cyclotron and the ring cyclotron were used to precess the proton spin polarization

into the horizontal plane so as to have either of the two spin states sideways ($\hat{x}$) or longitudinal ($\hat{z}$) on the target. Each magnet can rotate the direction of the polarization vector from the vertical to sideways direction. These solenoids are separated by two dipole magnets with a total bending angle of 45°, thus the solenoids allowed the delivery of the beam to the ring cyclotron with two different directions of the polarization vector in the horizontal plane. The spin precession angle in this dipole field is about 85° for 46.7 MeV protons. In this manner, we could provide a beam whose polarization axis was either in the $\hat{z}$ or $\hat{x}$ direction at the exit of the second solenoid by exciting the first or second solenoid, respectively. Single-turn extraction in the ring cyclotron was maintained to prevent depolarization of the horizontal component of the polarization vector. The extracted beam from the ring cyclotron was transported to the West Experimental Hall via the WS beamline [45]. The proton polarization was continuously measured with two beamline polarimeters separated by a total bending angle of 115°, precessing the spin of 250 MeV protons by about 260° between the two polarimeters. Both the horizontal and vertical components of the polarization vector were determined. During the measurements, typical values for polarization and beam current were 70% and 200 nA, respectively.

B. Calibration of the beamline polarimeter

Both beamline polarimeters consisted of four arms of collimated scintillation telescopes arranged in two pairs at conjugate angles. They are based on the analyzing power of $^1\mathrm{H}(\vec{p},p)^1\mathrm{H}$ scattering. Elastically scattered and recoil protons were detected in coincidence in a conjugate-angle pair at $\pm 17°$ and $\mp 70.9°$ on both sides of the beam. The solid angle of the pair of scintillators was 2.1 msr defined by a brass collimator in front of the backward scintillator. Both polarimeters used self-supporting polyethylene (CH_2) foils with a thickness of 1.3 mg/cm^2 as targets.

The analyzing powers of the polarimeters include contributions of the quasielastic $(\vec{p},2p)$ reaction on carbon nuclei whose analyzing power might be different from that of free *pp* scattering. The effective analyzing power of the polarimeter was determined by measurements of the analyzing power of the proton elastic scattering from ^{58}Ni at a laboratory angle of 18.75°. For the elastic scattering of spin-$\frac{1}{2}$ particles from spin-zero nuclei, there is a well-known relation between spin observables [46]

$$A_y^2 + R^2 + A^2 = 1, \tag{1}$$

where R and A are Wolfenstein parameters. When A_y is close to unity, its absolute value can be determined rather precisely from the measurements of R and A parameters even if they have relatively large uncertainties [46]. In this experiment, they were determined as

$$A = -0.145 \pm 0.02 \pm 0.004 \quad \text{and} \quad R = 0.071 \pm 0.02 \pm 0.002,$$

where the first and second errors are statistical and systematic, respectively. The systematic errors were estimated from uncertainties in the absolute values of the effective analyzing power of the FPP [47]. With these values, we obtained the analyzing power A_y to be 0.978 ± 0.004. The analyzing power of the beamline polarimeter was then determined to be 0.362 ± 0.003 at the laboratory angle of 17°.

C. Targets

Differential cross sections, analyzing powers, and a complete set of polarization transfer coefficients were measured for $\vec{p}d$ elastic scattering using self-supporting 99% isotopically enriched deuterated polyethylene foils (CD_2) with total thicknesses of 21 and 44 mg/cm^2. A 15-mg/cm^2-thick, natural carbon target was used to subtract contributions due to scattering on carbon. The CD_2 targets were produced by heating and pressing CD_2 powder [48]. To ensure constant D_2 target content during the experiment for angles larger than 25.5°, protons elastically scattered from deuterium were simultaneously measured by the LAS spectrometer set at a laboratory angle of 42.9°. Between measurements at smaller angles with the Grand Raiden, measurements were frequently repeated at the angle of 25.5°. The relative deviation of the target thickness was found to be constant within about $\pm 2.5\%$, which can be attributed to the inhomogenuity of CD_2 foils.

It is essential to get precise absolute cross sections for comparison with Faddeev calculations. Therefore, in a later measurement, a gaseous target was used to normalize cross sections taken with the solid CD_2 target. The gaseous target consisted of a cylinder of 40 mm diameter made of 200-μm-thick aluminum. The absolute gas pressure was continuously monitored by a barometer during measurements more precisely than 0.1%. The target cell was kept at room temperature and the temperature of the cell wall was measured during the experiment. The target cell was mounted on a target ladder, enabling quick change between either a solid target or a gaseous target. Spectra with filled and empty cells were measured to determine background contributions from the aluminum wall. A double-slit system was used to define the target volume and the solid angle of the Grand Raiden spectrometer. The effective target thickness and the solid angle were calculated by Monte Carlo simulations. In addition, a measurement was performed with hydrogen gas to check the system. The cross section of *pp* scattering at the laboratory angle of 25.5° was consistent within 3% with the value calculated by the phase-shift analysis program code SAID [49]. Independently, the thicknesses of solid CD_2 targets were also determined by normalizing the cross sections of the *pd* scattering at c.m. angles of 40°, 60°, and 95°.

D. Cross section and analyzing power measurements

Scattered protons or recoil deuterons in the *pd* scattering were momentum analyzed by the Grand Raiden spectrometer [39]. The horizontal and vertical acceptance of the Grand

Raiden was limited by a slit system to ± 20 and ± 30 msr, respectively. The LAS spectrometer was used to monitor the luminosity as described above. A slit system was used to limit the LAS acceptance to ± 50 and ± 60 msr in the horizontal and vertical plane, respectively. The focal plane counter system of each spectrometer consisted of two vertical drift chambers (VDC) and two ΔE plastic scintillators allowing ray reconstruction and the measurement of the particle time of flight (TOF) through the spectrometers. Each VDC consisted of pairs of x and u planes. In the off-line analysis, particle identification was performed using both ΔE and TOF measurements. Angular distributions were measured from 10° to 165° in 5° steps. A thin target (21 mg/cm^2) was used at forward angles up to 45°, and a thicker (44 mg/cm^2) target was used at larger angles. The ratio of the target thicknesses was determined by measurements with both targets at 40°. Protons were measured at angles smaller than 95°, and recoil deuterons at angles larger than 90°. At 90° and 95°, both protons and recoil deuterons were measured to verify the consistency. The yields from D_2 were obtained by subtracting contributions from carbon in the momentum spectra.

E. Polarization transfer measurements

The polarization of elastically scattered protons from CD_2 targets was measured at c.m. scattering angles from 10° to 95° by the FPP after momentum analysis in the Grand Raiden spectrometer. The FPP consisted of a thick carbon analyzer target, four multiwire proportional chambers, and large scintillator hodoscopes [40]. The effective analyzing power $A_y^{\rm eff}$ of the FPP was determined using the equation

$$A_y^{\rm eff}=\frac{\int \sigma^{\rm inc}(\theta)A_y^{\rm inc}(\theta)\cos\phi\, d\Omega}{\int \sigma^{\rm inc}(\theta)d\Omega}, \tag{2}$$

where $\sigma^{\rm inc}(\theta)$ and $A_y^{\rm inc}(\theta)$ are the differential cross section and the analyzing power for inclusive proton scattering from elastic, inelastic, and quasifree processes in the analyzer of the FPP. Angular integrations in Eq. (2) are performed over polar angles of $6° \leqslant \theta_{\rm lab} \leqslant 20°$ and azimuthal angles $|\phi_{\rm lab}| \leqslant 60°$. The inclusive cross section $\sigma^{\rm inc}(\theta)$ was measured in this experiment. The analyzing power $A_y^{\rm inc}(\theta)$ was parametrized as a function of the proton energy and scattering angle [50,51]. The thickness of the carbon analyzer was chosen to maximize the effective analyzing power that depends on the energy of the analyzed protons. It was 7 and 3 cm at the most forward and backward scattering angle, respectively.

The polarization transfer (PT) coefficients ($K_i^{j'}$) are defined by the following relation [46,52]:

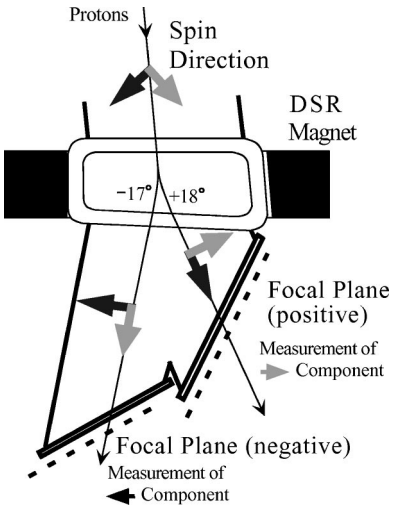

FIG. 2. Layout of the Grand Raiden dipole magnet for spin rotation (DSR).

$$\begin{pmatrix} p'_{x'} \\ p'_{y'} \\ p'_{z'} \end{pmatrix} = \frac{1}{1+p_y A_y}\left[\begin{pmatrix} 0 \\ P_{y'} \\ 0 \end{pmatrix} + \begin{pmatrix} K_x^{x'} & 0 & K_z^{x'} \\ 0 & K_y^{y'} & 0 \\ K_x^{z'} & 0 & K_z^{z'} \end{pmatrix} \begin{pmatrix} p_x \\ p_y \\ p_z \end{pmatrix} \right], \tag{3}$$

where p_i and p'_j, (i or $j=x,y,z$) denote the polarization of the incident and scattered protons, respectively. The coordinate system is defined in the Madison convention [53] in the laboratory frame. The off-diagonal elements of PT coefficients ($K_i^{j'}$) between the horizontal and vertical axes vanish due to parity conservation.

The proton spin precesses around the vertical axis of the spectrometer. The spin precession angle χ with respect to the momentum direction of the proton is described by $\chi = \gamma(g/2-1)\alpha$ in the moving frame, where γ is the Lorentz factor $\gamma=(m_pc^2+E_p)/m_pc^2$, g the spin g factor of the proton, which is related to the proton magnetic moment by $\mu_p = \frac{1}{2}g\mu_N$ (μ_N is the nuclear magneton), and α is the bending angle of the spectrometer. The total bending angle of the two dipole magnets of the Grand Raiden is 162° [39]. For the measurements of the proton polarization in the horizontal plane, a special dipole magnet for spin rotation (DSR) [54] was used to determine the two horizontal components of the polarization. The schematic layout of the DSR is shown in Fig. 2. The DSR is a dipole magnet just in front of the focal plane of the spectrometer, which bends protons through $+18°$ or $-17°$. The total bending angle of scattered protons along the central ray becomes 180° and 145° for the positive and negative polarities of the DSR, respectively. The vertical ($p'_{y''}$) and horizontal ($p'_{x''}$) components of the polarization are measured by the FPP. The spin precession angles of pro-

tons are expressed as $\chi^{(+)}$ and $\chi^{(-)}$ for the positive and negative polarities of the DSR, respectively. Then, the horizontal components of the polarization of the protons scattered by the CD_2 target are given by

$$p'_{y'} = p'_{y''}, \tag{4}$$

$$\begin{pmatrix} p'_{x'} \\ p'_{z'} \end{pmatrix} = \frac{1}{\sin(\chi^{(+)} - \chi^{(-)})} \times \begin{pmatrix} -\sin\chi^{(-)} & \sin\chi^{(+)} \\ \cos\chi^{(-)} & -\cos\chi^{(+)} \end{pmatrix} \begin{pmatrix} p'^{(+)}_{x''} \\ p'^{(-)}_{x''} \end{pmatrix}, \tag{5}$$

where $p'^{(+)}_{x''}$ and $p'^{(-)}_{x''}$ is measured with the positive and negative polarities of the DSR, respectively. In this experiment, the polarization of protons was measured between 120 MeV and 250 MeV. The spin precession angles ($\chi^{(+)}$, $\chi^{(-)}$) were (364°, 293°) and (409°, 329°) for 120 MeV and 250 MeV protons, respectively.

Measurements were performed using vertically polarized ($p_x = p_z = 0$) and horizontally polarized ($p_y = 0$) beams. At backward scattering angles larger than 45° in the c.m. frame, recoil deuterons were measured by the spectrometer LAS positioned at the conjugate angle in coincidence with protons detected by the Grand Raiden. This technique greatly reduced contributions of the scattering on carbon in the target. Differences in the particle TOF through the Grand Raiden and LAS spectrometers were used to obtain the number of coincidence events. Random coincidences were less than 1% of the total counts and were subtracted. At forward-scattering angles, measurements were also performed with the carbon target and contributions from carbon nuclei were subtracted in the momentum spectra.

III. THEORETICAL FORMALISM

We refer to Ref. [10] for a general overview on $3N$ scattering and its formulation as used here. We define an amplitude T in our main equation [55]

$$T = tP\phi + (1 + tG_0)V_4^{(1)}(1+P)\phi + tPG_0T + (1 + tG_0)V_4^{(1)}(1+P)G_0T. \tag{6}$$

The initial channel state ϕ occurring in the driving terms is composed of a deuteron and a momentum eigenstate of the projectile nucleon. The *NN* t operator is denoted by t, the free $3N$ propagator by G_0, and P is the sum of a cyclical and anticyclical permutation of three particles. The 3NF V_4 can always be described as a sum of three components

$$V_4 = V_4^{(1)} + V_4^{(2)} + V_4^{(3)}, \tag{7}$$

where $V_4^{(i)}$ is symmetrical under the exchange of the nucleons jk with $i \neq j \neq k$. As seen in Eq. (6) only one of three components occurs explicitly, the others enter implicitly via the permutations contained in P. The elastic scattering amplitude is given by

$$U = PG_0^{-1} + PT + V_4^{(1)}(1+P)\phi + V_4^{(1)}(1+P)G_0T. \tag{8}$$

The first term is the well-known single-particle exchange diagram. Then there are terms where either V_4 or the t's interact once. The remaining terms result from rescattering among the three particles. Again inserting the iteration of T as given in Eq. (6) into Eq. (8) yields a transparent insight [56]. After projecting onto a partial wave momentum space basis, Eq. (6) leads to a system of coupled integral equations, which can be solved numerically exactly for any nuclear force. In this study we restricted our partial wave basis to states with total angular momentum $j \leqslant 5$ in the two-nucleon subsystem. This corresponds to a maximum number of 142 partial wave states in the $3N$ system for a given total angular momentum and guarantees converged results for the elastic scattering observables at our energies. We verified the convergence by a comparison with results obtained when including $j = 6$ states, which increase the number of states to 194. This convergence check was done without 3NF. The inclusion of a 3NF was carried through for all total angular momenta of the $3N$ system up to $J = 13/2$ while the longer ranged $2N$ interactions require states up to $J = 25/2$. For details of the formalism and the numerical procedures we refer to Refs. [10,56,57].

In this paper we show calculations with various combinations of *NN* and $3N$ forces. The AV18, CD-Bonn, Nijm I, II, and 93 forces [1–3] are the *NN* forces. The TM, a modified version thereof labeled as TM′, and the Urbana IX forces are the 3NF's. We combined each of these *NN* interactions with the TM model [6,7], where the cutoff parameter Λ in the strong form factor parametrization was adjusted to reproduce the ^{3}H binding energy separately for each *NN* force [58]. The Λ values in units of the pion mass m_π are 5.215, 4.856, 5.120, 5.072, and 5.212 for AV18, CD-Bonn, Nijm I, II, and 93, respectively [59].

The standard parametrization of the TM 3NF has been criticized in Refs. [60–63], because it violates chiral symmetry. A form more consistent with chiral symmetry has been proposed by modifying the c term of the TM force and absorbing the long-range part of this term into the a term, leading to its new value $a' = a - 2m_\pi^2 c = -0.87/m_\pi$ [60–62], and rejecting the rest of the c term. This new form is called TM′ and the corresponding Λ value is $4.593 m_\pi$, when it is used with the CD-Bonn potential.

For the AV18 potential we also used the Urbana IX 3NF [8]. The force is based on the Fujita-Miyazawa assumption of an intermediate Δ excitation in the 2π exchange [9] and is augmented by a phenomenological spin- and isospin-independent short-range term. This force was formulated in configuration space [8]. For the partial-wave decomposition of the Urbana IX 3NF in momentum space we refer to Ref. [59].

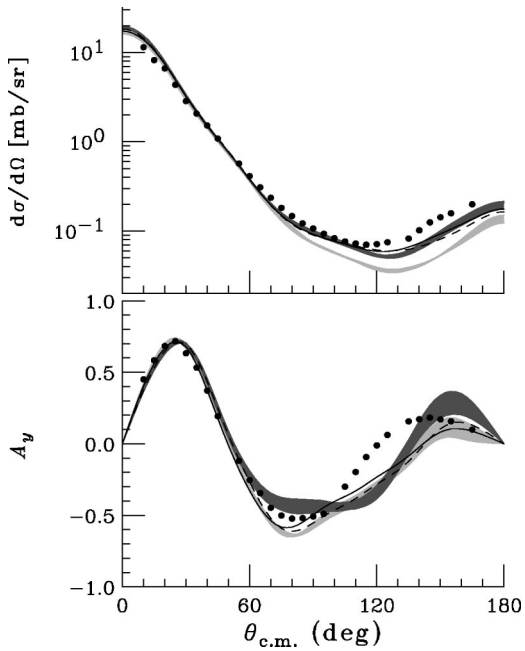

FIG. 3. The differential cross section $d\sigma/d\Omega$ (top) and proton analyzing powers (bottom) of elastic *pd* scattering at $E_p = 250$ MeV. The light shaded bands contain *NN* force predictions (AV18, CD-Bonn, Nijm I, II, and 93), the dark shaded bands contain the *NN*+TM 3NF predictions. The solid and dashed lines are the AV18+Urbana IX and CD-Bonn+TM′ predictions, respectively.

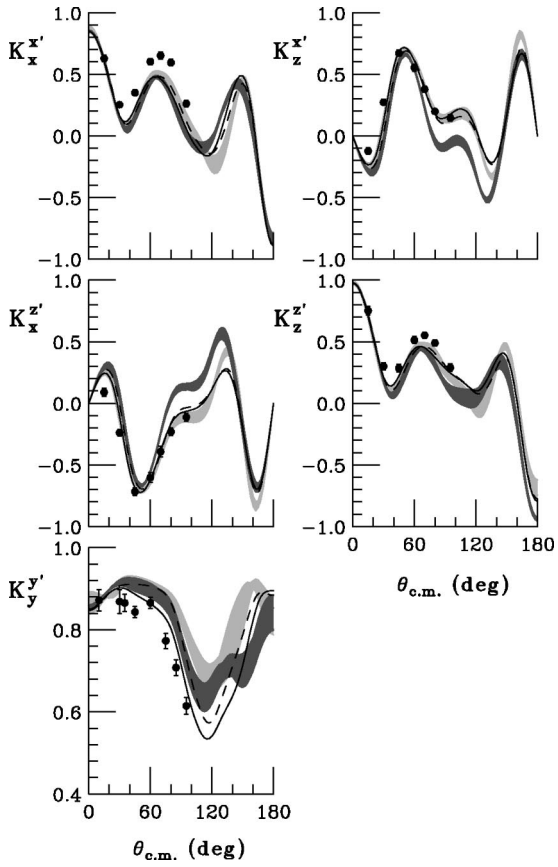

FIG. 4. Polarization transfer coefficients ($K_x^{x'}$, $K_x^{z'}$, $K_z^{x'}$, $K_z^{z'}$, and $K_y^{y'}$) of elastic *pd* scattering at $E_p = 250$ MeV. For the description of bands and lines see legend of Fig. 3.

IV. RESULTS AND DISCUSSION

The experimental results for the differential cross section ($d\sigma/d\Omega$), the vector analyzing power (A_y), and the PT coefficients ($K_x^{x'}$, $K_x^{z'}$, $K_z^{x'}$, $K_z^{z'}$, and $K_y^{y'}$) are shown in Figs. 3 and 4 and are tabulated in Tables I and II. The quoted errors are statistical ones only. The overall uncertainty in the absolute normalization of the cross section is estimated to be 3% from the calibration by the gaseous target measurements as previously described in Sec. II C. There is also the relative uncertainty of 2.5% attributed to the inhomogeneity of CD_2 foils. The analyzing power has an uncertainty of 1% in the absolute normalization owing to the precise calibration of the beamline polarimeter in this experiment. The PT coefficients have an uncertainty of 2.5% in the normalization [40]. For the PT coefficients, axes $\hat{i}$ and $\hat{j}'$ are defined in the laboratory scattering frame and $K_l^{j'}$ are plotted as function of the c.m. angles.

In the top panel of Fig. 3, the measured differential cross section is compared with theoretical predictions. The various 2NF predictions are very similar and are depicted by a narrow band (light shaded), which reflects the small dependence on the particular *NN* interaction used. The inclusion of the TM 3NF (dark shaded band) leads to a much better description at angles larger than 70°. This supports the claim of the clear evidence [14,17,64,65] of the 3NF from the systematic analysis of the energy dependence of the cross section data. The inclusion of the TM′ (dashed curve) and the Urbana IX (solid curve) 3NF's also leads to a good agreement to the data. However, discrepancies remain at angles larger than 120°. From the analysis of the $\vec{d}p$ data at the equivalent proton energy of 135 MeV [17], it has been shown that the TM 3NF and the Urbana IX 3NF provided a good description of the cross section even at very backward angles. In addition, at our energy of 250 MeV, both calculations with and without 3NF underestimate the data at forward angles (not visible on the scale of the figure) where the inclusion of the 3NF has little effect. The discrepancy between data and theoretical predictions, which increases with increasing energy [38], may be due to relativistic effects not accounted for in our nonrelativistic calculations.

In the bottom panel of Fig. 3, we compare the experimental analyzing power A_y with different nuclear-force predictions. The differences (narrow light shaded band) between the 2NF predictions are rather small at forward angles and become larger at backward angles. These predictions are in good agreement with the experimental data at forward angles, but deviate dramatically at backward angles larger than 60°. The experimental analyzing power A_y changes the sign at about 120°, while the calculations predict this change only around 140°. In the angular range 60°–120°, 2NF predictions are clearly larger in absolute value than experimental data. By including the TM 3NF (dark shaded band) the agreement with the data becomes better in the minimum around $\theta_{\rm c.m.} = 60°–100°$ but the discrepancies at more back-

TABLE I. Data of the *pd* elastic scattering cross sections and analyzing powers at 250 MeV.

$\theta_{\text{c.m.}}$ (deg)	$d\sigma/d\Omega$ (mb/sr)	$\Delta(d\sigma/d\Omega)$ (mb/sr)	A_y	$\Delta(A_y)$
10.0	11.450	0.060	0.451	0.008
15.0	8.220	0.034	0.584	0.006
20.0	6.634	0.026	0.684	0.006
25.0	4.342	0.014	0.717	0.005
30.0	2.853	0.009	0.633	0.005
35.0	2.066	0.006	0.533	0.004
40.0	1.525	0.004	0.372	0.003
45.0	1.087	0.003	0.193	0.004
55.0	0.571	0.004	−0.119	0.004
60.0	0.413	0.002	−0.254	0.006
65.0	0.309	0.001	−0.345	0.004
70.0	0.236	0.001	−0.447	0.004
75.0	0.182	0.001	−0.502	0.005
80.0	0.147	0.001	−0.523	0.005
85.0	0.122	0.001	−0.520	0.005
90.0	0.107	0.001	−0.509	0.004
95.0	0.093	0.001	−0.489	0.004
100.0	0.083	0.001		
105.0	0.076	0.001	−0.300	0.004
110.0	0.073	0.001	−0.197	0.004
115.0	0.070	0.001	−0.093	0.003
120.0	0.071	0.001	−0.011	0.003
125.0	0.075	0.001	0.062	0.003
135.0	0.082	0.001	0.157	0.004
140.0	0.102	0.001	0.172	0.004
145.0	0.125	0.001	0.183	0.004
150.0	0.143	0.001	0.171	0.004
155.0	0.158	0.001	0.158	0.005
165.0	0.199	0.001	0.099	0.004

ward angles remain. This is in contrast to the results for the deuteron vector analyzing power as shown in Ref. [17] where predictions with the TM 3NF describe the data very well not only in the minimum, but also at backward angles. The present result is consistent with the proton analyzing powers measured at 200 MeV at IUCF [18]. Calculations with the TM′ (dashed curve) or Urbana IX 3NF (solid curve) do not improve the agreement with the data.

Our PT data are shown in Fig. 4 together with theoretical predictions. The PT coefficients in the horizontal plane ($K_x^{x'}$, $K_x^{z'}$, $K_z^{x'}$, and $K_z^{z'}$) are reasonably well described by calculations with 2NF only (light shaded bands). The inclusion of the TM 3NF (dark shaded bands) rather deteriorates the agreement with the experimental data. The TM′ (dashed curves) and the Urbana IX (solid curves) 3NF do not have a large effect on these PT coefficients and give a reasonably good agreement with the data. In the case of the PT coefficient in the vertical plane ($K_y^{y'}$), the inclusion of the TM 3NF (dark shaded band) and especially the Urbana IX 3NF (solid curve) give results in better agreement with the measurements. This is similar to the case of the analyzing power, which is also a polarization observable in the vertical plane. These results clearly indicate that the spin-dependent parts of 3NF's are not well described in present-day models.

Our measurements were limited to relatively forward angles $\theta_{\text{c.m.}} \leqslant 95°$. In Fig. 4, large differences are observed between theoretical predictions with and without 3NF's at more backward angles for some PT coefficients. At angles larger than 100°, the energies of scattered protons are less than 120 MeV where the present FPP at the Grand Raiden has a poor efficiency [40]. A low-energy FPP is now under development at the RCNP to enable measurements of proton polarization below 120 MeV. This will permit measurements to better constrain the proper spin structure of 3NF's and to study the significance of relativity.

V. SUMMARY AND CONCLUSION

A complete set of polarization transfer coefficients was measured at 250 MeV proton energy for $\vec{p}d$ elastic scattering together with precise cross section and proton analyzing power angular distributions covering a wide range of angles from 10° to 165°. The target consisted of CD_2 (deuterated polyethylene) foils. Precise absolute normalization of the cross sections was achieved by independent measurements with a gaseous target. The uncertainty in the overall normal-

TABLE II. Data of proton polarization transfer coefficients of the *pd* elastic scattering at 250 MeV.

$\theta_{\text{c.m.}}$ (deg)	$K_x^{x'}$	$\Delta(K_x^{x'})$	$K_x^{z'}$	$\Delta(K_x^{z'})$	$K_z^{x'}$	$\Delta(K_z^{x'})$	$K_z^{z'}$	$\Delta(K_z^{z'})$	$K_y^{y'}$	$\Delta(K_y^{y'})$
10.0									0.871	0.026
15.0	0.629	0.028	0.089	0.034	−0.123	0.028	0.752	0.034		
30.0	0.253	0.022	−0.239	0.026	0.272	0.023	0.300	0.029	0.868	0.029
35.0									0.865	0.021
45.0	0.350	0.023	−0.717	0.031	0.671	0.026	0.284	0.028	0.843	0.014
60.0	0.603	0.025	−0.602	0.041	0.554	0.029	0.513	0.029	0.865	0.013
70.0	0.653	0.029	−0.392	0.042	0.378	0.026	0.552	0.024		
75.0									0.773	0.019
80.0	0.594	0.027	−0.231	0.030	0.199	0.020	0.489	0.024		
85.0									0.708	0.020
95.0	0.261	0.027	−0.113	0.033	0.146	0.026	0.289	0.032	0.614	0.021

ization was estimated to be 3% by comparing *pp* scattering data with calculations by the phase-shift analysis program code SAID. There is also the relative uncertainty of 2.5%. The beamline polarimeters were calibrated carefully to give the small uncertainty of 1% in the normalization for the analyzing power of the *pp*-scattering data at $\theta_{\mathrm{lab.}}=17°$ with a CH_2 target.

The present data were compared with predictions based on different nuclear forces in order to search for 3NF effects. Based on the comparison of our data with pure $2N$ force predictions, clear discrepancies have been found for most observables. For the cross section, these discrepancies at intermediate angles can be removed by including any 3NF used in the present study, the TM 3NF, its modified version called TM′, and the Urbana IX 3NF. At backward angles, the inclusion of the 3NF's significantly reduces the discrepancies, but is not sufficient to explain the data completely. While one can probably neglect *pp*-Coulomb force effects at the present energy [66], it is very likely that relativistic effects play a role. Such a behavior is also found for the proton analyzing power. The PT coefficients are very sensitive to the inclusion of the TM 3NF to give worse descriptions of the data except for $K_y^{y'}$. For the PT coefficients in the horizontal plane ($K_x^{x'}$, $K_x^{z'}$, $K_z^{x'}$, and $K_z^{z'}$) calculations with the TM′ and Urbana IX 3NF provide predictions similar to those with 2NF only and a better description of the data. On the other hand, predictions of the PT coefficient in the vertical plane ($K_y^{y'}$) are improved by all three 3NF models, where Urbana IX comes closest to the data. Overall, these results clearly indicate that the spin structure of 3NF's is not properly described by present models.

At intermediate energies, our data are the first complete set of PT coefficients for $\vec{p}d$ elastic scattering covering a wide angular range and serve as a good testing ground of the investigation of the spin structure of 3NF's and the effects of relativity. In order to offer further valuable sources of information, a rich spectrum of spin observables will be measured not only for elastic scattering, but also for the *Nd* breakup process. For both of them, large 3NF effects have been predicted at higher energies [67,68].

ACKNOWLEDGMENTS

We thank the RCNP staff for their support during the experiment. We also wish to thank Professor H. Toki for his encouragements throughout the work. We are grateful to Dr. G.P.A. Berg for his critical reading of the manuscript. This experiment was performed under Program No. E146 and R38 at the RCNP. This work was supported in part by the Grant-in-Aid for Scientific Research No. 14340074 of the Ministry of Education, Culture, Sports, Science and Technology of Japan, and NSF Grant No. PHY0070858. The numerical calculations have been performed on the Cray SV1 and T3E of the NIC in Jülich, Germany.

[1] R.B. Wiringa, V.G.J. Stoks, and R. Schiavilla, Phys. Rev. C **51**, 38 (1995).
[2] R. Machleidt, F. Sammarruca, and Y. Song, Phys. Rev. C **53**, R1483 (1996).
[3] V.G.J. Stoks, R.A.M. Klomp, C.P.F. Terheggen, and J.J. de Swart, Phys. Rev. C **49**, 2950 (1994).
[4] A. Nogga, H. Kamada, and W. Glöckle, Phys. Rev. Lett. **85**, 944 (2000).
[5] A. Nogga, H. Kamada, W. Glöckle, and B.R. Barrett, Phys. Rev. C **65**, 054003 (2002).
[6] S.A. Coon, M.D. Scadron, P.C. McNamee, B.R. Barrett, D.W.E. Blatt, and B.H.J. McKellar, Nucl. Phys. **A317**, 242 (1979); S.A. Coon and W. Glöckle, Phys. Rev. C **23**, 1790 (1981); S.A. Coon, Few-Body Syst., Suppl. **1**, 41 (1984); S.A. Coon and J.L. Friar, Phys. Rev. C **34**, 1060 (1996).
[7] S.A. Coon and M.T. Peña, Phys. Rev. C **48**, 2559 (1993).
[8] B.S. Pudliner, V.R. Pandharipande, J. Carlson, Steven C. Pieper, and R.B. Wiringa, Phys. Rev. C **56**, 1720 (1997).
[9] J. Fujita and H. Miyazawa, Prog. Theor. Phys. **17**, 360 (1957).
[10] W. Glöckle, H. Witała, D. Hüber, H. Kamada, and J. Golak, Phys. Rep. **274**, 107 (1996).
[11] A. Kievsky, M. Viviani, and S. Rosati, Phys. Rev. C **64**, 024002 (2001).
[12] J.L. Friar, B.F. Gibson, G. Berthold, W. Glöckle, Th. Cornelius, H. Witała, J. Haidenbauer, Y. Koike, G.L. Payne, J.A. Tjon, and W.M. Kloet, Phys. Rev. C **42**, 1838 (1990).
[13] S.C. Pieper, V.R. Pandharipande, R.B. Wiringa, and J. Carlson, Phys. Rev. C **64**, 014001 (2001).
[14] H. Witała, W. Glöckle, D. Hüber, J. Golak, and H. Kamada, Phys. Rev. Lett. **81**, 1183 (1998).
[15] E. Epelbaum *et al.* (unpublished).
[16] S. Nemoto, K. Chmielewski, S. Oryu, and P.U. Sauer, Phys. Rev. C **58**, 2599 (1998); S. Nemoto, K. Chmielewski, U. Meyer, J. Haidenbauer, S. Oryu, and P.U. Sauer, Few-Body Syst. **24**, 241 (1998).
[17] K. Sekiguchi, H. Sakai, H. Witała, W. Glöckle, J. Golak, M. Hatano, H. Kamada, H. Kato, Y. Maeda, J. Nishikawa, A. Nogga, T. Ohnishi, H. Okamura, N. Sakamoto, S. Sakoda, Y. Satou, K. Suda, A. Tamii, T. Uesaka, T. Wakasa, and K. Yako, Phys. Rev. C **65**, 034003 (2002).
[18] E.J. Stephenson, H. Witała, W. Glöckle, H. Kamada, and A. Nogga, Phys. Rev. C **60**, 061001(R) (1999).
[19] K. Ermisch, A.M. van den Berg, R. Bieber, W. Glöckle, J. Golak, M. Hagemann, V.M. Hannen, M.N. Harakeh, M.A. de Huu, N. Kalantar-Nayestanaki, H. Kamada, M. Kiš, J. Kuroś-Żołnierczuk, M. Mahjour-Shafiei, A. Micherdzińska, A. Nogga, R. Skibiński, H. Witała, and H.J. Wörtche, Phys. Rev. Lett. **86**, 5862 (2001).
[20] W.P. Abfalterer, F.B. Bateman, F.S. Dietrich, Ch. Elster, R.W. Finlay, W. Glöckle, J. Golak, R.C. Haight, D. Hüber, G.L. Morgan, and H. Witała, Phys. Rev. Lett. **81**, 57 (1998).
[21] H. Witała, H. Kamada, A. Nogga, W. Glöckle, Ch. Elster, and D. Hüber, Phys. Rev. C **59**, 3035 (1999).
[22] S.K. Adhikari, L. Tomio, and T. Frederico, Phys. Rev. C **48**, 2105 (1993).

[23] A. Stadler, F. Gross, and M. Frank, Phys. Rev. C **56**, 2396 (1997).
[24] J.L. Forest and V.R. Pandharipande, Phys. Rev. C **60**, 014002 (1999).
[25] H. Mineo, W. Bentz, and K. Yazaki, Phys. Rev. C **60**, 065201 (1999).
[26] Z. Papp, A. Krassnigg, and W. Plessas, Phys. Rev. C **62**, 044004 (2000).
[27] W. Glöckle, T.-S.H. Lee, and F. Coester, Phys. Rev. C **33**, 709 (1986).
[28] H. Kamada and W. Glöckle, Phys. Rev. Lett. **80**, 2547 (1998).
[29] H. Kamada, Few-Body Syst., Suppl. **12**, 433 (2000).
[30] H. Shimizu, K. Imai, N. Tamura, K. Nisimura, K. Hatanaka, T. Saito, Y. Koike, and Y. Taniguchi, Nucl. Phys. **A382**, 242 (1982).
[31] S.P. Wells, S.W. Wissink, A.D. Bacher, S.M. Bowyer, S. Chang, J. Lisantti, J. Liu, C. Olmer, A.K. Opper, T. Rinckel, and E.J. Stephenson, Nucl. Instrum. Methods Phys. Res. A **325**, 205 (1993).
[32] M. Poulet, A. Michalowicz, K. Kuroda, and D. Cronenberger, Nucl. Phys. **A99**, 442 (1967).
[33] H. Postma and R. Wilson, Phys. Rev. **121**, 1229 (1961).
[34] K. Kuroda, A. Michalowicz, and M. Poulet, Nucl. Phys. **88**, 33 (1966).
[35] R.E. Adelberger and C.N. Brown, Phys. Rev. D **5**, 2139 (1972).
[36] H. Rühl, B. Dechant, J. Krug, W. Lübcke, G. Spangardt, G. Spangardt, M. Steinke, M. Stephan, D. Kamke, J. Balewski, K. Bodek, L. Jarczyk, A. Stuzałakowski, W. Hajdak, St. Kistryn, R. Müller, J. Lang, R. Henneck, H. Witała, Th. Cornelius, and W. Glöckle, Nucl. Phys. **A524**, 377 (1991).
[37] R.V. Cadman, J. Brack, W.J. Cummings, J.A. Fedchak, B.D. Fox, H. Gao, W. Glöckle, J. Golak, C. Grosshauser, R.J. Holt, C.E. Jones, H. Kamada, E.R. Kinney, M.A. Miller, W. Nagengast, A. Nogga, B.R. Owen, K. Rith, F. Schmidt, E.C. Schulte, J. Sowinski, F. Sperisen, E.L. Thorsland, R. Tobey, J. Wilbert, and H. Witała, Phys. Rev. Lett. **86**, 967 (2001).
[38] H. Rohdjeß, W. Scobel, H.O. Meyer, P.V. Pancella, S.F. Pate, M.A. Pickar, R.E. Pollock, B.v. Przewoski, T. Rinckel, F. Sperisen, H. Witała, J. Golak, D. Hüber, H. Kamada, and W. Glöckle, Phys. Rev. C **57**, 2111 (1998).
[39] M. Fujiwara, H. Akimune, I. Daito, H. Fujimura, Y. Fujita, K. Hatanaka, H. Ikegami, I. Katayama, K. Nagayama, N. Matsuoka, S. Morinobu, T. Noro, M. Yoshimura, H. Sakaguchi, Y. Sakemi, A. Tamii, and M. Yosoi, Nucl. Instrum. Methods Phys. Res. A **422**, 484 (1999).
[40] M. Yosoi, H. Akimune, I. Daito, M. Fujiwara, S. Hirata, T. Inomata, O. Kamigaito, M. Kawabata, T. Noro, Y. Sakemi, T. Takahashi, A. Tamii, S. Toyama, A. Yamagoshi, M. Yoshimura, and H. Sakaguchi, in *High Energy Spin Physics*, edited by K. J. Heller and S. L. Smith, AIP Conf. Proc. No. 343 (AIP, Woodbury, NY, 1995), p. 157.
[41] N. Matsuoka, T. Noro, K. Sagara, S. Morinobu, A. Okihana, and K. Hatanaka, RCNP report, 1992.
[42] K. Hatanaka, K. Takahisa, H. Tamura, M. Sato, and I. Miura, Nucl. Instrum. Methods Phys. Res. A **384**, 575 (1997).
[43] I. Miura, T. Yamazaki, A. Shimizu, K. Hosono, T. Itahashi, T. Saito, A. Ando, K. Tamura, K. Hatanaka, M. Kibayashi, M. Uraki, H. Ogata, M. Kondo, and H. Ikegami, in *Proceedings of the 13th International Conference on Cyclotrons and their Applications, Vancouver, 1992*, edited by G. Dutto and M. K. Craddock (World Scientific, Singapore, 1993), p. 3.
[44] H. Sakai, H. Okamura, H. Otsu, T. Wakasa, S. Ishida, N. Sakamoto, T. Uesaka, Y. Satou, S. Fujita, and K. Hatanaka, Nucl. Instrum. Methods Phys. Res. A **369**, 120 (1996).
[45] T. Wakasa, K. Hatanaka, Y. Fujita, G.P.A. Berg, H. Fujimura, H. Fujita, M. Itoh, J. Kamiya, T. Kawabata, K. Nagayama, T. Noro, H. Sakaguchi, Y. Shimbara, H. Takeda, K. Tamura, H. Ueno, M. Uchida, M. Uraki, and M. Yosoi, Nucl. Instrum. Methods Phys. Res. A **482**, 79 (2002).
[46] G.G. Ohlsen, Rep. Prog. Phys. **35**, 717 (1972).
[47] D. Hirooka, M.Sc. thesis, Osaka University, 2001.
[48] Y. Maeda, H. Sakai, K. Hatanaka, and A. Tamii, Phys. Rev. C (to be published).
[49] R. A. Arndt and L. D. Roper, *Scattering Analysis Interactive Dial-In Program* (SAID), phase-shift solution SP98, Virginia Polytechnic Institute and State University (unpublished); see also Phys. Rev. C **56**, 3005 (1997), and references therein.
[50] M.W. McNaughton, B.E. Bonner, H. Ohnuma, O.B. Van Dijk, Sun Tsu-Hsun, C.L. Hollas, D.J. Cremans, K.H. McNaughton, P.J. Riley, R.F. Rodebaugh, Shen-Wu Xu, S.E. Turpin, B. Aas, and G.S. Weston, Nucl. Instrum. Methods Phys. Res. A **241**, 435 (1985).
[51] T. Kawabata, H. Akimune, G.P.A. Berg, H. Fujimura, H. Fujita, Y. Fujita, M. Fujiwara, K. Hara, K. Hatanaka, K. Hosono, T. Ishikawa, M. Itoh, J. Kamiya, M. Nakamura, T. Noro, E. Obayashi, H. Sakaguchi, Y. Shimbara, H. Takeda, T. Taki, A. Tamii, H. Toyokawa, M. Uchida, H. Ueno, T. Wakasa, K. Yamasaki, Y. Yasuda, H.P. Yoshida, and M. Yosoi, Phys. Rev. C **65**, 064316 (2002).
[52] N. Hoshizaki, J. Phys. Soc. Jpn. **55**, 549 (1986), and references therein.
[53] S. E. Darden, in *Proceedings of the Third International Symposium on Polarization Phenomena in Nuclear Reactions, Madison, 1970*, edited by H. H. Barschall and W. Haeberli (The University of Wisconsin Press, Madison, 1971), p. 39.
[54] M. Fujiwara, S. Morinobu, M. Yosoi, and H. Ikegami, in *Proceedings of the Internatioal Conference on Heavy Ion Research with Magnetic Spectrographs, Michigan State University, East Lansing, 1989*, edited by N. Anantaraman and B. Sherrill, National Superconducting Cyclotron Laboratory Technical Report No. MSUCL-685, p. 283.
[55] D. Hüber, H. Kamada, H. Witała, and W. Glöckle, Acta Phys. Pol. B **28**, 1677 (1997).
[56] D. Hüber, H. Witała, and W. Glöckle, Few-Body Syst. **14**, 171 (1993).
[57] H. Witała, Th. Cornelius, and W. Glöckle, Few-Body Syst. **3**, 123 (1988).
[58] A. Nogga, D. Hüber, H. Kamada, and W. Glöckle, Phys. Lett. B **409**, 19 (1997).
[59] H. Witała, W. Glöckle, J. Golak, A. Nogga, H. Kamada, R. Skibiński, and J. Kuroś-Żołnierczuk, Phys. Rev. C **63**, 024007 (2001).
[60] J.L. Friar, D. Hüber, and U. van Kolck, Phys. Rev. C **59**, 53 (1999).
[61] D. Hüber, J.L. Friar, A. Nogga, H. Witała, and U. van Kolck, Few-Body Syst. **30**, 95 (2001).

[62] H. Kamada, D. Hüber, and A. Nogga, Few-Body Syst. **30**, 121 (2001).
[63] S.A. Coon and H.K. Han, Few-Body Syst. **30**, 131 (2001).
[64] N. Sakamoto, H. Okamura, T. Uesaka, S. Ishida, H. Otsu, T. Wakasa, Y. Satou, T. Niizeki, K. Katoh, T. Yamashita, K. Hatanaka, Y. Koike, and H. Sakai, Phys. Lett. B **367**, 60 (1996).
[65] H. Sakai, K. Sekiguchi, H. Witała, W. Glöckle, M. Hatano, H. Kamada, H. Kato, Y. Maeda, A. Nogga, T. Ohnishi, H. Okamura, N. Sakamoto, S. Sakoda, Y. Satou, K. Suda, A. Tamii, T. Uesaka, T. Wakasa, and K. Yako, Phys. Rev. Lett. **84**, 5288 (2000).
[66] Y. Maeda, H. Sakai, K. Hatanaka, H. Okamura, A. Tamii, T. Wakasa, K. Yako, K. Sekiguchi, S. Sakoda, J. Kamiya, K. Suda, H. Kato, M. Hatano, D. Hirooka, T. Saito, N. Uchigashima, M.B. Greenfield, and J. Rapaport, in *Spin 2000*, edited by K. Hatanaka, T. Nakano, K. Imai, and H. Ejiri, AIP Conf. Proc. No. 570 (AIP, Melville, NY, 2001), p. 719.
[67] H. Witała, W. Glöckle, H. Kamada, A. Nogga, J. Golak, J. Kuroś-Żołnierczuk, and R. Skibiński, in *Spin 2000* (Ref. [66]).
[68] J. Kuroś-Żołnierczuk, H. Witała, J. Golak, H. Kamada, A. Nogga, R. Skibiński, and W. Glöckle, nucl-th/0203017; nucl-th/0203020 (to be published in Phys. Rev. C).